Scintillation and spectroscopic properties of Ce 3+−doped YAlO 3 and Lu x(RE) 1−xAlO 3(RE=Y 3+ and Gd 3+) scintillators

ARTICLE *in* NUCLEAR INSTRUMENTS AND METHODS IN PHYSICS RESEARCH SECTION A ACCELERATORS SPECTROMETERS DETECTORS AND ASSOCIATED EQUIPMENT · FEBRUARY 2003

Impact Factor: 1.22 · DOI: 10.1016/S0168-9002(02)01996-4

Available online at www.sciencedirect.com
SCIENCE DIRECT®
Nuclear Instruments and Methods in Physics Research A 498 (2003) 312–327
NUCLEAR INSTRUMENTS & METHODS IN PHYSICS RESEARCH Section A
www.elsevier.com/locate/nima

Scintillation and spectroscopic properties of Ce^{3+}-doped $YAlO_3$ and $Lu_x(RE)_{1-x}AlO_3$($RE = Y^{3+}$ and Gd^{3+}) scintillators

J.A. Mares[a,*], M. Nikl[a], N. Solovieva[a], C. D'Ambrosio[b], F. de Notaristefani[c], K. Blazek[d], P. Maly[d], K. Nejezchleb[d], P. Fabeni[e], G.P. Pazzi[e], J.T.M. de Haas[f], C.W.E. van Eijk[f], P. Dorenbos[f]

[a] *Institute of Physics, Academy of Sciences of the Czech Republic, Cukrovarnicka 10, 16253 Prague 6, Czech Republic*
[b] *CERN, EP Division, CH-1211 Geneve 23, Switzerland*
[c] *INFN, Sezione di Roma, Rome, Italy*
[d] *Crytur Limited, Palackeho 175, 51101 Turnov, Czech Republic*
[e] *IFAC-CNR, via Panciatichi 64, I-50127 Florence, Italy*
[f] *Radiation Technology Group, Interfaculty Reactor Institute, Delft University of Technology, Mekelweg 15, 2629 JB Delft, The Netherlands*

Received 18 June 2002; received in revised form 12 November 2002; accepted 19 November 2002

Abstract

Scintillation properties like photoelectron yield and light yield of Ce^{3+}-doped $YAlO_3$ and mixed $Lu_x(RE)_{1-x}AlO_3$ ($RE = Y^{3+}$ and Gd^{3+}) perovskite crystals are presented. The photoelectron yields increase almost linearly with γ-ray energy but a small non-linearity is observed around 40 keV. Scintillation and spectroscopic properties like UV or X-ray excited emission, laser excited emission, excitation and absorption spectra and photo- and scintillation decay of the different crystals are compared. The influence of intrinsic absorption and reflecting tape on the yields are discussed. Selected $YAlO_3$:Ce showed the highest light yield of 25,000 phels/MeV and an energy resolution of 4.5% for 662 keV γ-radiation. The γ-ray linear absorption coefficient increases with Lu content and that of $LuAlO_3$:Ce is almost 10 times higher than that of $YAlO_3$:Ce.

PACS: 78.40.Ha; 78.55.Hx; 78.60.Kn

Keywords: $YAlO_3$:Ce and $Lu_x(RE)_{1-x}AlO_3$:Ce scintillators; Scintillation; Photoelectron yield; Light yield; Spectroscopic properties

1. Introduction

Recently, various new and improved inorganic scintillators have been investigated [1–14] with the goal to find heavy, fast, and more efficient materials with high light yield and energy

*Corresponding author. Tel.: +420-2-203-18542; fax: +420-2-333-43184.
E-mail address: amares@fzu.cz (J.A. Mares).

0168-9002/03/$ - see front matter
PII: S0168-9002(02)01996-4

resolution for applications in X- and γ-ray radiation detectors [15–20]. Applications include medical imaging, industrial systems like security systems at airports, X-ray astronomy, etc. The heavy and fast but low light yield $PbWO_4$ (PWO) scintillator has been chosen for the new generation of electromagnetic calorimeters of the CMS and ALICE experiments at the LHC project at CERN [21]. Various Ce^{3+}-doped scintillators, especially compounds with ABO_3 perovskite structure have been developed and tested as multi-detectors in γ-imaging cameras or as improved modules for positron emission tomography (PET) systems [16,17,22–24].

Generally, new or improved inorganic scintillating crystals or glasses used in modern applications should fulfill the following conditions: (i) high scintillation photoelectron yield $N_{phels}(E)$ at energy E or a photon light yield LY exceeding 20,000 photons/MeV [1,5,15,25–27]; (ii) fast scintillation decay with lifetimes in the range of tens of ns together with low afterglow, i.e., slow ms decay components should not be present; (iii) high-effective atomic mass Z_{eff} for efficient X- or γ-ray absorption resulting in good stopping power in the energy range 5 keV to 1 MeV; (iv) large Stokes shift between $f \rightarrow d$ absorption and $d \rightarrow f$ emission [1,28] and (v) good mechanical and chemical properties, especially stability in severe environmental conditions.

At present, photo, X- or γ-ray excited emission spectra, excitation or absorption spectra, and luminescence decay of crystals investigated are well known. Results by different laboratories on scintillators compare well [1,5,8–10]. However, other properties as the photoelectron yield or photon yields reported by different laboratories may differ up to several tens of percent [9,10,15]. This imposes a problem, when results on scintillating crystals reported by different researchers are to be compared.

Recent light yield measurements have shown that substantial improvement can be reached if small and around 1 mm thin samples are investigated [25]. The correction factors needed to convert photoelectron yields $N_{phels}(E)$ into photon light yield LY include: (i) light collection efficiency (CE) of scintillating photons on the photon detector; (ii) CE of generated photoelectrons in the photo-multiplier tube (PMT); (iii) quantum efficiency of PMT detectors and also (iv) processes inside crystals during X- or γ-ray irradiation like self-absorption, presence of traps or quenching centers, etc. [9,25]. A new development in scintillation measurements started after Hybrid Photomultiplier Tubes (HPMT) were introduced [26,27].

A classical LY measurement set-ups consist of: (1) a γ-ray source like ^{137}Cs 662; (2) a front-end PMT like Philips XP 2020Q; (3) a sample placed in good optical contact by means of silicon oil with the PMT-window; and (4) an electronic detection system. The sample is usually covered by a few layers of Teflon tape to ensure good reflection of scintillating photons into the photo-cathode [1,5,11–14]. The generated signals from PMTs are measured mainly with shaping amplifiers.

Recently, the HPMT were developed [26] and they introduce a new tool for scintillation $N_{phels}(E)$ photoelectron yield measurements. The HPMT consists of an entrance window with the photo-cathode evaporated on its inner side and a small silicon diode placed opposite to the center of the photo-cathode that acts as anode. These electrodes together with the focusing electrodes are sealed in a vacuum tube. The Si-diode detects the electrostatically focused electrons liberated from the photo-cathode [26,27]. Generally, the HPMT set-up can measure $N_{phels}(E)$ in a linear range of about four orders of magnitude [29,30]. Another substantial improvement of HPMT was obtained by replacing the quartz photo-cathode window by a $YAlO_3$:Ce (YAP:Ce) scintillator [26,27]. This replacement yields improved light transmission from scintillator into HPMT. For $Bi_4Ge_3O_{12}$ (BGO) the response increased by a factor of 1.78 as compared to that with an HPMT with quartz window [27].

A scintillating photo-cathode window as $YAlO_3$:Ce [27] or other crystals should fulfill properties like high hardness, non-hygroscopicity, mechanical and chemical stability and good optical and scintillation properties. A small disadvantage of $YAIO_3$:Ce is the low density of 5.36 g/cm^3 and small Z_{eff} of 34 [5].

The aim of this paper is to use a HPMT with quartz photo-cathode window for characterizing

Table 1
Properties of the $YAlO_3$:Ce samples {abbr. YAP:Ce (RS), YAP:Ce(i) and YAP1-11}. Dimension, Ce concentration, the slopes of scintillation photoelectron yield {ΔN_{phels}(ave)} and the estimated photoelectron yield N_{phels}(estim) are compiled. Top and bottom faces of the samples were polished while their sides were grounded (no reflection tape was used). Samples from YAP2 to YAP11 are Zr co-doped $YAlO_3$:Ce crystals

Crystal sample	Dimension (mm^3)	Ce conc. (at%)	ΔN_{phels}(ave) (phels/keV)	N_{phels}(estim) (phels/MeV)	Light yield (ph/MeV)
YAP:Ce(RS)	$9\times7\times1$	0.11	1.63	3260	13,040
YAP:Ce(RS)	$9\times7\times2$	0.11	1.85	3700	14,800
YAP:Ce(RS)	$9\times7\times5$	0.11	1.55	3100	12,400
YAP:Ce(RS)	$9\times7\times9$	0.11	1.35	2700	10,800
YAP:Ce(1)	$7\times5\times2$	0.54	1.11	2220	8,880
YAP:Ce(2)	$7\times5\times2$	0.47	2.19	4380	17,520
YAP:Ce(3)	$7\times5\times2$	0.45	1.72	3440	13,760
YAP:Ce(4)	$7\times5\times2$	0.26	1.66	3320	13,280
YAP1(no Zr)	$7\times7\times1$	0.11	2.69	5380	21,520
YAP2	$7\times7\times1$	0.14	2.55	5100	20,400
YAP3	$7\times7\times1$	0.12	2.68	5360	21,440
YAP4	$7\times7\times1$	0.13	2.7	5400	21,600
YAP5	$7\times7\times1$	0.17	1.52	3040	12,160
YAP6	$7\times7\times1$	0.33	1.94	3880	15,520
YAP7	$7\times7\times1$	0.27	2.62	5240	20,960
YAP8	$7\times7\times1$	0.31	1.98	3960	15,840
YAP9	$7\times7\times1$	0.52	1.69	3380	13,520
YAP10	$7\times7\times1$	0.45	2.4	4080	16,320
YAP11	$7\times7\times1$	0.32	2.25	4500	18,000

and comparing $N_{phels}(E)$ photoelectron yields of newly developed or improved $YAlO_3$:Ce and $Lu_x(RE)_{1-x}AlO_3$:Ce ($RE=Y^{3+}$ and Gd^{3+}) pure and mixed perovskite scintillators. Their $N_{phels}(E)$ will be discussed together with other important properties like the density, Z_{eff}, Stokes shift, decay time, etc. Finally, linear attenuation coefficients for $YAlO_3$:Ce, Lu_xY_{1-x} $YAlO_3$:Ce and pure $LuAlO_3$:Ce were calculated and presented for energies up to 1 MeV.

2. Experimental

2.1. Samples and their preparation

Scintillation and spectroscopic properties of various $YAlO_3$:Ce and $Lu_x(RE)_{1-x}AlO_3$:Ce ($RE=Y^{3+}$, Gd^{3+}) scintillating crystals were investigated together with a BGO crystal. $YAlO_3$:Ce and $Lu_x(RE)_{1-x}AlO_3$:Ce crystals belong to the group of distorted perovskite crystals with orthorhombic structure [5]. All perovskite crystals and BGO were grown by the Czochralski method in the same company.[1] Details on the composition and description of samples investigated will be presented in Tables 1–4 further in the text.

Most samples are cylindrical with 8 mm diameter and 1, 2, 5 or 10 mm thickness. Other samples were rectangular of about $7\times7\times1$ or $\times2\,mm^3$ dimension. Top and bottom faces of the samples were polished to average optical quality but their cylindrical walls or sides were grounded. For luminescence and absorption measurements mainly samples of 1 mm thickness were used.

From $YAlO_3$:Ce crystal with the highest quality and efficiency new well defined $YAlO_3$:Ce samples were prepared. These samples will be referred as samples SKB11A01/861, 858 and 862. They are cylindrical with 10 mm diameter and 1, 2 and 10 mm thickness. Top and bottom faces of these samples were polished up to average optical quality but their cylindrical walls were grounded.

[1] The crystals were grown by the company Crytur Ltd., Palackeho 175, 51101 Turnov, Czech Republic.

Table 2
Characteristics of $Lu_xY_{1-x}AlO_3$:Ce, $Lu_xGd_{1-x}AlO_3$:Ce and BGO crystals. Dimension, Ce concentrations, the slopes of scintillation photoelectron yield $\{\Delta N_{phels}(ave)\}$ and the estimated photoelectron yield $N_{phels}(estim)$ are compiled. Top and bottom faces of the samples were polished while their cylindrical walls were grounded (no reflection tape was used). $Lu_{0.1}Y_{0.9}$ means $Lu_{0.1}Y_{0.9}AlO_3$:Ce, $Lu_{0.6}$ $Gd_{0.4}$ means $Lu_{0.6}Gd_{0.4}AlO_3$:Ce, etc. Correction factor of BGO photoelectron yield to compare with the perovskite samples is 1.25

Sample	Dimension (mm^3)	Ce conc. (at%)	ΔN_{phels}(ave) slopes (phels/keV)	N_{phels}(estim) (phels/MeV)	Light yield (ph/MeV)
$Lu_{0.1}Y_{0.9}$	∅ 8×1	0.15	1.94	3880	15,520
$Lu_{0.1}Y_{0.9}$	∅ 8×2	0.15	1.79	3580	14,320
$Lu_{0.1}Y_{0.9}$	∅ 8×5	0.15	1.33	2660	10,640
$Lu_{0.2}Y_{0.8}$	∅ 8×1	0.12	1.64	3280	13,120
$Lu_{0.2}Y_{0.8}$	∅ 8×2	0.12	1.35	2700	10,800
$Lu_{0.2}Y_{0.8}$	∅ 8×5	0.12	1.28	2560	10,240
$Lu_{0.3}Y_{0.7}$	∅ 8×1	0.19	1.74	3480	13,920
$Lu_{0.3}Y_{0.7}$	∅ 8×2	0.19	1.6	3200	12,800
$Lu_{0.3}Y_{0.7}$	∅ 8×5	0.19	1.38	2760	11,040
$Lu_{0.65}Y_{0.35}$	∅ 8×1	0.13	1.67	3340	13,360
$Lu_{0.65}Y_{0.35}$	∅ 8×2	0.13	1.55	3100	12,400
$Lu_{0.65}Y_{0.35}$	∅ 8×5	0.13	1.45	2900	11,600
$Lu_{0.6}Y_{0.4}$	$8\times6\times2$	0.27	1.48	2960	11,840
BGO	∅ 8×1	—	0.625	1250	5000
BGO	∅ 8×2	—	0.5125	1025	4100
BGO	∅ 8×5	—	0.525	1050	4200

Table 3
Characteristics of $Lu_xY_{1-x}AlO_3$:Ce, and $Lu_xGd_{1-x}AlO_3$:Ce. Dimension, Ce concentrations, photoelectron yield $N_{phels}(E)$ at 511 keV, the slopes of scintillation yield $\{\Delta N_{phels}(ave)\}$ and the estimated photoelectron yield $N_{phels}(estim)$ are compiled. Top and bottom faces of the samples were polished while their sides were grounded. The samples were covered by several layers of Teflon tape. Sample description is the same as in Table 2

Sample	Size-shape (mm^3)	Ce conc. (at%)	N_{phels} at 511 keV	ΔN_{phels}(ave) slopes (phels/keV)	N_{phels}(estim) (phels/MeV)	Light yield (ph/MeV)
$Lu_{0.1}Y_{0.9}$	∅ 8×10	0.15	775	1.52	3040	12,160
$Lu_{0.2}Y_{0.8}$	∅ 8×10	0.12	658	1.29	2580	10,320
$Lu_{0.3}Y_{0.7}$	∅ 8×10	0.19	795	1.56	3120	12,480
$Lu_{0.65}Gd_{0.35}$	∅ 8×10	0.13	860	1.68	3360	13,440

Table 4
Results of pulse height measurements with a PMT of selected and efficient $YAlO_3$:Ce crystals (sample names SKB11A01/861, 858 and 862) under 662 keV ^{137}Cs γ-radiation. Top and bottom faces of the samples were polished while their cylindrical walls were grounded. The samples were covered by several layers of Teflon tape. Samples were of various thicknesses and yields with different shaping times were measured

YAP:Ce samples investigated (mm^3)	Shaping time (μs)	N_{phels} (phels/MeV)	Light yield (ph/MeV)	Resolution (%)
∅ 10×1	3	6601	23760	4.6
∅ 10×1	10	6874	24750	4.6
∅ 10×2	3	6557	23600	5.0
∅ 10×2	10	6818	24550	5.2
∅ 10×10	3	4547	16370	6
∅ 10×10	10	4725	17000	6.1

2.2. Spectroscopic and laser excited emission measurements

Ce^{3+} emission and excitation spectra and fluorescence decay was measured by a fluorescence spectrometer Model 199S Edinburgh Instruments [5]. 511 keV γ-rays from a ^{22}Na was used for the scintillation decay measurements [7]. Absorption spectra were measured either by a spectrophotometer Model Shimadzu UV3101PC [31] or by a Hewlett-Packard HP 8452A [12–14]. X-ray induced emission spectra were carried out with a Philips PW 2253/20 X-ray tube with Cu anode at 35 kV. The measurements were performed in reflection mode and the spectra have been corrected for the sensitivity of the photon detection system.

Laser excited Ce^{3+} emission spectra of the selected 10 mm long $YAlO_3$:Ce SKB crystal and 5 mm long $Lu_{0.3}Y_{0.7}AlO_3$:Ce and $Lu_{0.65}Gd_{0.35}AlO_3Ce$ crystals were measured under excitation by the 308 nm line of a XeCl pulsed laser. The effect or re-absorption of luminescence on the emission spectra was measured as function of the laser excitation spot position. The samples were placed with the cylindrical axis perpendicular to the pencial-shape excitation beam. By means of a copper plate with three holes, i.e., near the beginning (position A), at the center (position B) and near the end (position C) for $YAlO_3$:Ce. The two positions B and C were used for mixed perovskite crystals. The positions of the holes will be sketched in Figs. 9 and 10 in the following sections. The Ce^{3+} emission around 365 nm was observed through the top or bottom face of the cylindrical samples by means of a Jobin-Yvon Triax 320 spectrometer and recorded by a model EG&G-PARC 1240 multi-channel analyzer. The intensity of 308 nm laser line excitation was 8 kW/mm^2 with a repetition rate of 10 Hz and pulse width of 10 ns.

2.3. $N_{phels}(E)$ photoelectron yield measurements

The $N_{phels}(E)$ photoelectron yield was measured with the set-up described in Refs. [26,27]. The set-up shown in Fig. 1 consists of the HPMT[2] with a quartz photo-cathode window of 40 mm active diameter and with up to 13 or 15 kV accelerating voltage between the photo-cathode and the anode. X- or γ-ray line sources were placed roughly 0.5–2 cm above the surface of the scintillating sample. The samples were placed in the center of the outer face of the photo-cathode window and optically coupled to it with silicon oil.

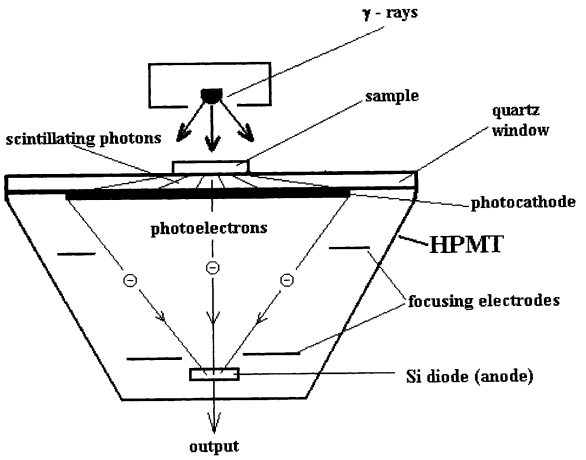

Fig. 1. Scheme of $N_{phels}(E)$ scintillation photoelectron yield measurement with HPMT.

We used a variable X-and γ-ray source emitting characteristic X- or γ-rays at 8.16 keV (Cu), 13.6 keV (Rb), 17.8 keV (Mo), 22.6 keV (Ag), 32.9 keV (Ba) and 44.5 keV (Tb) (all these lines are excited by 59.5 keV γ-ray line of ^{241}Am). ^{57}Co (122 keV), ^{109}Cd (22.6 keV) and ^{22}Na (511 keV) γ-ray lines were also used as individual γ-ray sources. The obtained signals were electronically processed by spectroscopic techniques [26,27].

The photoelectron yield $N_{phels}(E)$ is determined from the ration between the position of total X- or γ-ray absorption peak and the position of the single photoelectron or multi-photoelectron peak. In the case of PMT measurements a proper correction or gain differences in the measuring electronics was made.

Depending on the scintillation decay of the crystal, an appropriate spectroscopic shaping time must be selected. For Ce^{3+}-doped perovskites and the BGO crystal we mainly used 1 or 2 μs shaping time because their scintillation lifetimes are

[2] HMPT was assembled by DEP (Delft Elektronische Produkten), NL-9300AB Roden, The Netherlands.

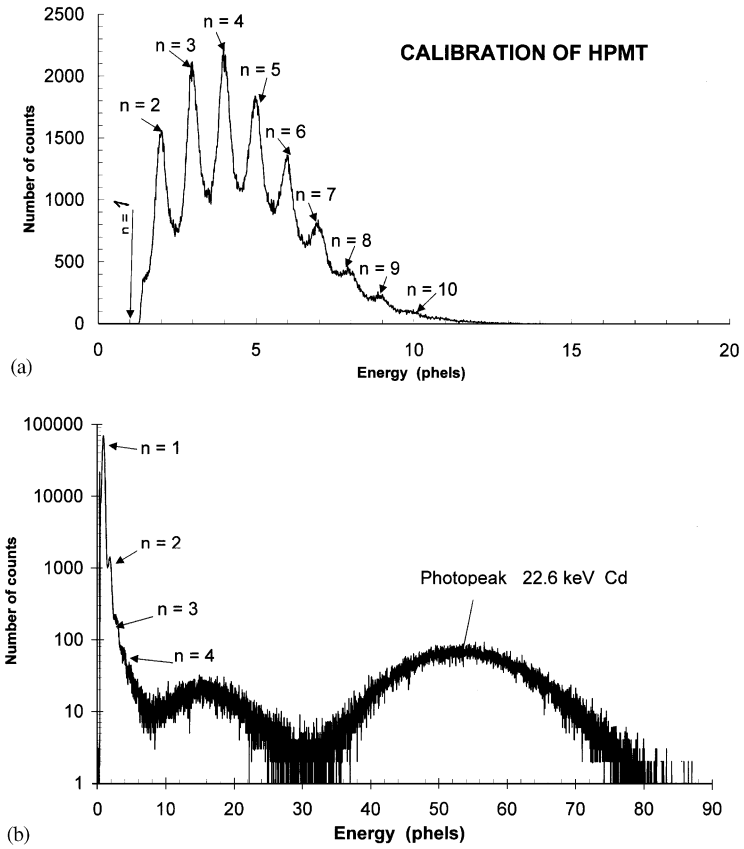

Fig. 2. (a) Pulse height spectrum of single photoelectrons and multi-photoelectrons detected with an HPMT. (b) Pulse height spectrum of ^{109}Cd X-ray source with the 1 mm thick $YAlO_3$:Ce, Zr (YAP11) sample. 1 μs spectroscopic shaping time was used and the gain is 1000 times at HV = 13 kV. The electronic noise is ≈2.6 keV.

$\tau_{sc} \approx 20-30$ ns and 300 ns, respectively [5]. For the majority of perovskite crystals investigated the slow components comprise 10–15% of the total scintillation pulse [2,4,5].

We measured $N_{phels}(E)$ with and without reflecting tape placed immediately above the sample. Especially, Tyvec tape was used [26,29]. A circular Tyvec sheet of 30 mm in diameter was immediately above the samples for reflecting the scintillating photons back to the photo-cathode of the HPMT. With this tape N_{phels} increased by 45–50% compared to the situation without Tyvec tape. However, for the measurements presented in this paper we decided not to use Tyvec reflection tape from the point of view of a possible application of these crystals for scintillating windows in HPMTs or ISPA tubes [27] or as pixels in $YAlO_3$:Ce multi-detectors [17].

Different from a PMT there are no dynodes in an HPMT. Single or multi-photoelectrons ejected from the photo-cathode can then be detected separately by the Si-diode as anode. This can be seen from a calibration curve in Fig. 2(a). It provides a means to calibrate the HPTM. Fig. 2(b) shows an example of a pulse height spectrum measured with $YAlO_3$:Ce on the HPTM showing the 22.6 keV photo-peak of the X-ray line from ^{109}Cd. The single photoelectron ($n = 1$) and two photoelectron ($n = 2$), etc. detection can be seen clearly.

For comparing the different samples, it is important that they have roughly the same shape

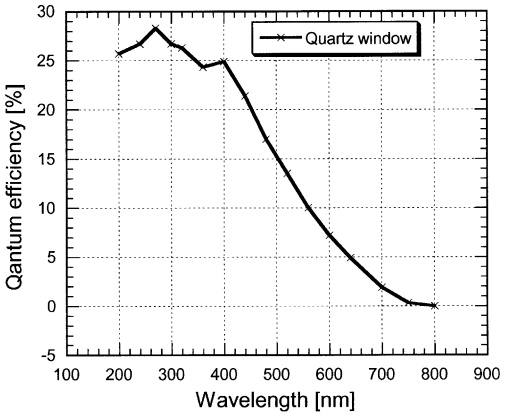

Fig. 3. The S20 photo-detection quantum efficiency of the used HPMT.

and dimension, are polishing to the same degree and show the same Ce^{3+} emission band peaking around 370 nm [3–5,31]. To compare BGO with the perovskite samples it is necessary to make a correction for its different emission spectrum in the blue–green range by employing the quantum efficiency curve of the HPMT photo-cathode shown in Fig. 3. The photoelectron yields of BGO must be multiplied by an estimated correction factor of ≈ 1.25.

The reproducibility of N_{phels} measurements was checked with two samples measured at different times with the same set-up. The results show differences of $\pm 2.5\%$ or $\pm 3.5\%$ which falls within the estimated less than 5% accuracy in determining $N_{phels}(E)$ [26,27].

2.4. Light yield measurements of selected $YAlO_3$:Ce crystal (SKB samples)

Light yields measurement under ^{137}Cs 662 keV γ-ray excitation, of high quality and efficient $YAlO_3$:Ce SKB crystals of 10 mm diameter and 1, 2 and 10 mm diameter and 1, 2 and 10 mm thick samples were carried out at the laboratory in Delft [12–14]. Top and bottom of the samples were polished but their cylindrical sides are grounded. The samples were covered with a few layers of 0.1 mm thick Teflon tape and mounted on a Hamamatsu PMT tube R1791 with viscasil oil for good optical coupling. We also checked the reflection of Teflon tape, which is in the UV range of Ce^{3+} emission roughly constant. The photoelectron yield is obtained from the quotient of the channel position of the maximum of the full energy peak and the channel position of the maximum in the single photoelectron peak. With the quantum efficiency of the used PMT and the measured emission spectrum, the LY in photons/MeV was calculated.

3. Experimental results

3.1. $N_{phels}(E)$ yields of $YAlO_3$:Ce and $Lu_x(RE)_{1-x}AlO_3$:Ce (Re=Y^{3+} and Gd^{3+}) crystals

The perovskite $YAlO_3$:Ce and $Lu_x(RE)_{1-x}AlO_3$:Ce (RE = Y^{3+} and Gd^{3+}) crystals were prepared from different crystal boules. The studied groups of samples are listed below:

1. Various $YAlO_3$:Ce crystal samples of almost similar shape and dimension, (see Table 1) with Ce concentrations ranging from ≈ 0.1 to 0.55 at%. Also Zr co-doped $YAlO_3$:Ce samples of dimensions $7 \times 7 \times 1\,mm^3$ were investigated.
2. $Lu_xY_{1-x}AlO_3$:Ce samples, see Tables 2 and 3, with $x = 0.1$, 0.2 and 0.3 of cylindrical shape with diameter 8 mm and thickness 1, 2, 5 or 10 mm. Their Ce concentration ranges between 0.12 and 0.19 at%. [5].
3. $Lu_xGd_{1-x}AlO_3$:Ce samples with $x = 0.6$ and 0.65. Dimensions are $8 \times 6 \times 2\,mm^3$ for $x = 0.6$ and for $x = 0.65$ the samples are cylindrical with diameter 8 mm and thickness 1, 2, 5 or 10 mm, see Tables 2 and 3. Their Ce concentrations are 0.27 and 0.13 at% for $x = 0.6$ or 0.65, respectively [5].
4. One BGO crystal (prepared by the Crytur company, see[1]) was measured for comparison with the perovskite samples from groups 1, 2 and 3. Samples were cylindrical with diameter 8 mm and thickness 1, 2, 5 and 10 mm. The appearance of the crystals from groups 1–4 is always good and not many scattering centers or defects are visible. The $Lu_xGd_{1-x}AlO_3$:Ce samples, however, contain clearly visible defects like cracks and bubbles. The photoelectron

yields $N_{phels}(E)$ was measured up to 122 keV (^{57}Co γ-line) and occasionally up to 511 keV (^{22}Na γ-line).

All measured samples from groups 1–3 exhibit up to 122 keV or even up to 511 keV an almost linear dependence of $N_{phels}(E)$ with energy E as shown in Figs. 4–6. The same is valid for BGO. On almost all samples measured, $N_{phels}(E)$ decreases with sample thickness. The highest photoelectron yields $N_{phels}(E)$ and consequently also the highest photon light yields LY were mostly observed for 1 mm thick samples, see Tables 1–4. However, for the $YAlO_3$:Ce {YAP:Ce(RS) sample} the highest yield is observed for the 2 mm thick sample, see Table 1. For the selected $YAlO_3$:Ce SKB crystal almost the same yields are obtained for 1 and 2 mm thick samples, see Table 4.

Photoelectron yields $N_{phels}(E)$ increase linearly with energy up to 500 keV, but we can distinguish roughly two ranges where these dependences are not the same. For example the $YAlO_3$:Ce,Zr (YAP11 sample) in the energy range from 5 to 40 keV, the slope of $N_{phels}(E)$ is ≈2.5 phels/keV (ph/keV), while in the higher energy range above 40 keV the slope is ≈2.25 phels/keV. For another $YAlO_3$:Ce,Zr (YAP6 sample) crystal the slope is ≈2.03 phels/keV up to 40 keV while in the higher energy range up to 1 MeV the slope is ≈1.94 phels/keV. Generally, a proportional $N_{phels}(E)$ dependence on Ce concentration was not observed, see Tables 1–3.

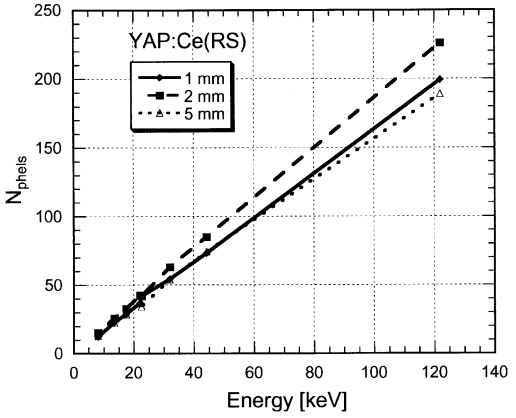

Fig. 4. $N_{phels}(E)$ photoelectron yield as function of the energy measured with $YAlO_3$:Ce {YAP:Ce(RS) sample} of different thickness derived from X- and γ- ray total absorption peaks in the range 5–122 keV.

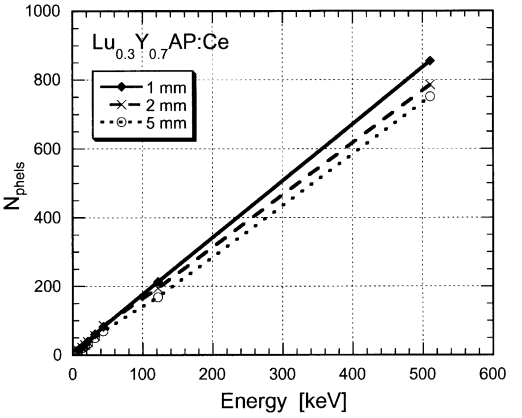

Fig 5. $N_{phels}(E)$ photoelectron yield as function of the energy measured with $Lu_{0.3}Y_{0.7}AlO_3$:Ce samples of different thickness derived from X- and γ-ray total absorption peaks in the range 5–600 keV.

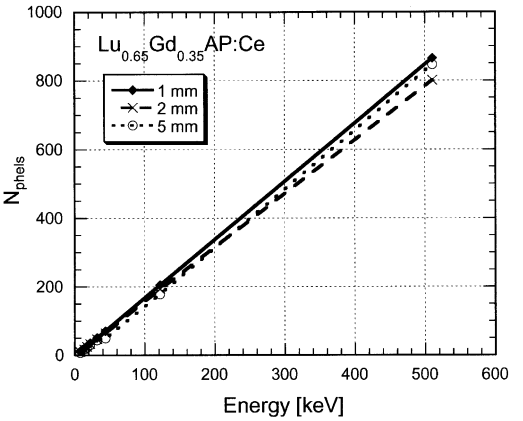

Fig. 6. $N_{phels}(E)$ photoelectron yield as function of the energy measured with $Lu_{0.65}Gd_{0.35}AlO_3$:Ce samples of different thickness derived from X- and γ-ray total absorption peaks in the range 5–600 keV.

$N_{phels}(E)$ of $YAlO_3$:Ce crystals at one specific energy may vary up to 30%, see Fig. 7 where, the results on various $YAlO_3$:Ce crystals prepared at different times are presented. This Figure demonstrates that N_{phels} is probably influenced

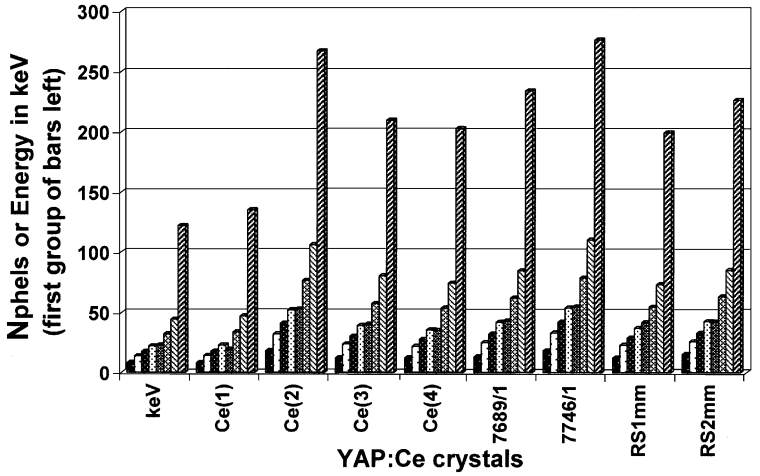

Fig. 7. $N_{phels}(E)$ photoelectron yield as function of the energy of total absorption peaks for very different $YAlO_3$:Ce crystals (prepared at different times). The bars in the left of the diagram show the energies of X- and γ-ray total absorption lines in the range 5–122 keV that were used.

by the growth method, purity of raw materials or dopants, temperature variations during crystal growth, quality of seeds or post-growth annealing.

3.2. Pulse height measurements on good quality and efficient $YAlO_3$:Ce (SKB) crystal

We selected the most efficient $YAlO_3$:Ce crystal (SKB samples) characterized by high optical quality and luminescence efficiency. Pulse height measurements using the method described in Section 2.4 were carried out on samples of 1, 2 and 10 mm thickness. The photoelectron yields $N_{phels}(E)$ and photon yield LY are presented in Table 4. The highest LYs are obtained with 1 and 2 mm thick samples, see Fig. 8. For the 10 mm thick sample, LY decreased to roughly 70% of the value for thin samples. Scintillation decay measurements of these selected $YAlO_3$:Ce SKB crystals, performed at the Delft University of Technology set-up described in Refs. [12–14], indicated two exponential decay components. A fast one with $\tau = 20$ ns and a slow one with $\tau = 25$ μs. The presence of the slow component is reflected as a 4 % increase of LY when the shaping time increases from 3 to 10 μs, see Table 4.

3.3. Scintillation and optical properties of $YAlO_3$:Ce and $Lu_x(RE)_{1-x}AlO_3$:Ce ($RE = Y^{3+}$ and Gd^{3+}) crystals

Emission and excitation spectra of $YAlO_3$:Ce and $Lu_x(RE)_{1-x}AlO_3$:Ce ($RE = Y^{3+}$ and Gd^{3+}) crystals were measured in the near UV range under lamp and laser excitation at room (RT) and liquid nitrogen (LNT) temperature. Ce^{3+} emission spectra are roughly the same, i.e., a wide emission band peaking around 370 nm. Only small differences were observed in the Ce^{3+} luminescence excitation spectra. A long wavelength tail in the range 320–350 nm in the excitation spectrum overlaps with the short wavelength tail in the emission spectrum.

Fig. 9 shows laser excited ($\lambda_{ex} = 308$ nm) Ce^{3+} emission spectra of $YAlO_3$:Ce (SKB sample $\varnothing$ $10 \times 10\,mm^2$). The sample was excited at the beginning, center and at the end of the crystal. Near the short wavelength side, the spectra depend on the position of excitation spot. The integral of the emission spectrum at points B and C are 5.6% and 10.8% smaller than that at point A. For the 5 mm thick $Lu_{0.3}Y_{0.7}AlO_3$:Ce sample in Fig. 10 the intensity at point B is 11.6% smaller than at the beginning at point C. For $Lu_{0.65}Gd_{0.35}AlO_3$:Ce the difference is 16.7%.

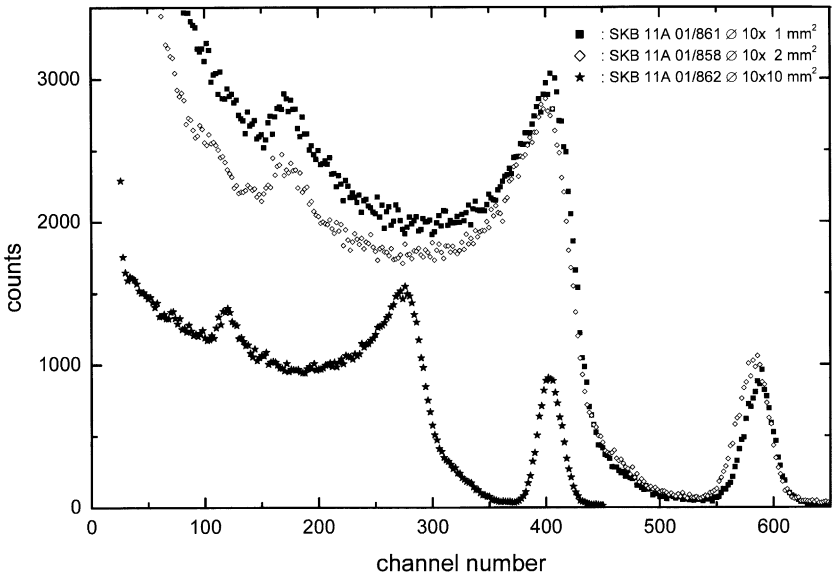

Fig. 8. Pulse height measurement of high quality and efficient $YAlO_3$:Ce SKB crystals of diameter 10 mm and of thickness 1, 2 and 10 mm measured with a ^{137}Cs γ-ray source (662 keV energy) and photo-multiplier readout.

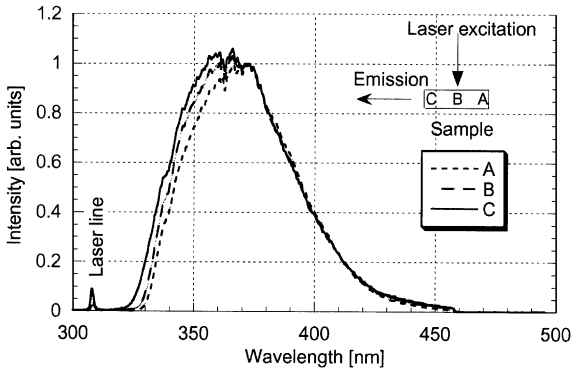

Fig. 9. Room temperature emission spectra from the 10 mm long $YAlO_3$:Ce SKB crystal. The crystal was excited with the 308 nm XeCl line of a laser at points A, B and C on the crystal cylindrical side.

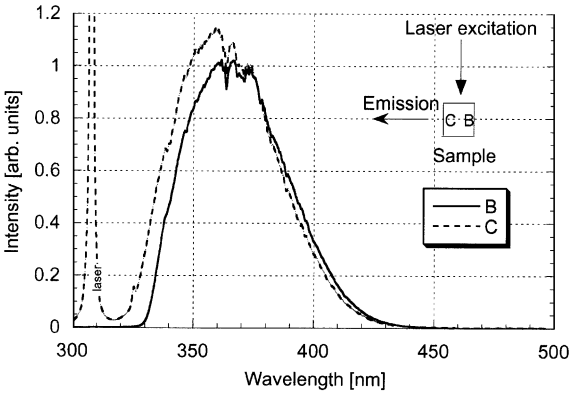

Fig. 10. Room temperature emission spectra from the 5 mm long $Lu_{0.3}Y_{0.7}AlO_3$:Ce crystal. The crystal was excited with the 308 nm XeCl line of a laser at points B and C on the crystal cylindrical side.

Details on the Ce^{3+} emission spectra of the crystals investigated and $LuAlO_3$:Ce are summarized in Table 5. The highest value for the Stokes shift measured at LNT is observed for $YAlO_3$:Ce ($\approx 4132\,cm^{-1}$) and the lowest value for $Lu_{0.3}Y_{0.7}AlO_3$:Ce ($\approx 2875\,cm^{-1}$). Almost the same applies for the spin orbit splitting between the $^2F_{5/2}$ and $^2F_{7/2}$ levels of Ce^{3+} where the highest value was observed for $LuAlO_3$;Ce and $YAlO_3$:Ce (a bit above $2000\,cm^{-1}$) and the smallest one for $Lu_{0.65}Gd_{0.35}AlO_3$:Ce($\approx 1422\,cm^{-1}$).

The X-ray excited emission spectrum of $YAlO_3$:Ce SKB is shown in Fig. 11, together with transmission spectra of the crystals with 1 and 10 mm thickness. Again, one observes the overlap between Ce^{3+} absorption and emission spectra. Above 350 nm the transmission has a constant value of 80 %. This high transmission points to the

Table 5
Optical properties of Ce^{3+} emission and excitation of pure and mixed perovskites at $T = 80$ K

Crystal	λ_{em} (cm^{-1}) (peak of $^2F_{5/2}$)	FWHM (cm^{-1})	ΔS (cm^{-1})	Δ ($^2F_{5/2}$–$^2F_{7/2}$) (cm^{-1})
$YAlO_3$:Ce(RS)	344.41	4029	4132	2095
$LuAlO_3$:Ce	348.53	4515	3881	2120
$Lu_{0.3}Y_{0.7}AlO_3$:Ce	≈350	4037	2875	1617
$Lu_{0.65}Gd_{0.35}AlO_3$:Ce	≈352.65	4006	4006	1422

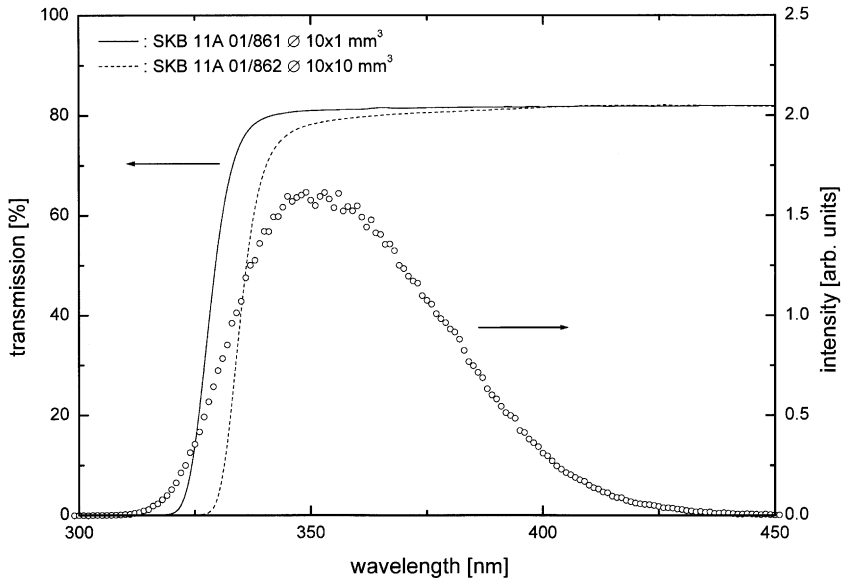

Fig. 11. Room temperature transmission spectra of 1 and 10 mm thick $YAlO_3$:Ce SKB crystals together with (open circles) the X-ray excited emission spectrum.

high quality of the $YAlO_3$:Ce crystals. For the studied $Lu_x(RE)_{1-x}AlO_3$:Ce (RE = Y^{3+} or Gd^{3+}) crystals the transmission above 350 nm is around 50%.

4. Discussion

4.1. Photoelectron yields $N_{phels}(E)$ of the crystals

The photoelectron yield $N_{phels}(E)$ [25] should be proportional to the scintillation light yield $N_{ph}(E)$ which is the number of photons produced in the scintillator at given energy E. $N_{phels}(E)$ can be expressed as

$$N_{phels}(E) \propto N_{ph}(E) \times \eta_1 \times QE \times \varepsilon, \quad (1)$$

where η_1 is the light CE, QE the quantum efficiency of the photo-cathode averaged over the emission spectrum of the scintillator, and ε the efficiency of photoelectron collection on the anode of the PMT or HPMT. In our experimental set-up where we use HPMT, see Fig. 1, $\eta_1 \times \varepsilon$ can be expressed as the total CE. The surface areas of the samples are between 50 and 100 mm^2. Since this is much smaller than the active area of 1250 mm^2 of the HPMT photo-cathode surface, almost all scintillation photons going down enter the photo-cathode and will contribute to photo-electron generation. The arrangement of the HPMT causes that generated photoelectrons are focused and detected by the Si diode as anode. $N_{phels}(E)$ measured with HPMT can be written as $\propto N_{ph}(E) \times QE \times CE$.

Because all measured perovskite samples exhibit almost the same emission spectrum we may compare their $N_{phels}(E)$ without making corrections for the QE curve of HPMT given in Fig. 3. To compare with BGO a correction factor of ≈ 1.25 due to its different emission spectrum has to be used. Finally, for perovskite crystals $N_{phels}(E)$ is given simply by $\propto N_{ph}(E) \times$ Corr. Fact. $(= QE(\lambda) \times CE)$.

With the HPMT we detect photoelectrons generated by scintillating photons propagating down from the γ-interaction spot on samples into the HPMT. They should represent roughly 40 % of the total number of generated scintillating photons under assumption that Ce^{3+} emission is isotropic. If one would have used reflecting tape, the $N_{phels}(E)$ yield at given energy should be at least two times higher than that measured without the reflecting tape. For samples of dimensions $\varnothing\ 8 \times 1\,mm^3$ we can assume that $\approx$20–30% of the scintillating photons emerge through the cylindrical wall and roughly 35–40% and 35–40% through the top and bottom face, respectively. The estimated (total) photoelectron yields N_{phels}(estim) expected at 1 MeV excitation were calculated from the average slopes of ΔN_{phels}(ave) in the $N_{phels}(E)$ versus E curves and are given in the 4th and 5th columns of Tables 1 and 2 and in the 5th and 6th columns of Table 3. The LY per MeV was calculated from N_{phels}(estim) and the quantum efficiency $\approx$25% of the HPMT at $\lambda_p = 370$ nm of Ce^{3+} emission peak. The LY per MeV are given in the last columns of Tables 1–3. Based on the above expressions and according to measuring conditions, scintillation characteristics $N_{phels}(E)$, LY(E) of samples and spectroscopic properties were compiled.

4.2. $N_{phels}(E)$ yields of $YAlO_3$:Ce and $Lu_x(RE)_{1-x}AlO_3$:Ce ($RE = Y^{3+}$ and Gd^{3+}) crystals

At present $YAlO_3$:Ce crystals exhibit the highest photoelectron yields from the different perovskite group of crystals investigated in the energy range 5 keV to 1 MeV. The highest $N_{phels}(E)$ values were obtained with samples of 1 or 2 mm thickness, see Tables 1, 4 and Figs. 7 and 12. In that energy range the yields increase linearly with energy, see Fig. 4. $N_{phels}(E)$ yields decrease with increase of sample thickness, see Fig. 12. $N_{phels}(E)$ exhibit linear dependence with E but there are two ranges where their slopes $\{\Delta N_{phels}(E) = N_{phels}(E)/E\}$ are different. Above $\approx$ 40 keV the slopes are about similar as the values ΔN_{phels}(ave) in Tables 1–3. Below $\approx$40 keV the slopes are somewhat larger.

In the last 11 rows of Table 1 and in Fig. 7 (samples numbers 7689/1 and 7746/1) $N_{phels}(E)$ yields of Zr co-doped $YAlO_3$:Ce crystals are presented. All samples have the same dimension and shape and are polished similarly. $N_{phels}(E)$ at 122 keV is up to 60% higher than previously grown $YAlO_3$:Ce [YAP:Ce(RS)] or similar $YAlO_3$:Ce crystals (see Table 1). In the series of $YAlO_3$:Ce, Zr (YAP1 untill YAP11) crystals [32] the highest $N_{phels}(E)$ yields were observed for the YAP3 and YAP4 crystal. These crystals are characterized by relatively low Ce concentrations around 0.12 at%. Again within the whole $YAlO_3$:Ce, Zr crystal series no clear dependence of $N_{phels}(E)$ on Ce concentration is observed.

The mixed $Lu_xY_{1-x}AlO_3$:Ce or $Lu_xGd_{1-x}AlO_3$:Ce perovskite crystals also exhibit linear dependences of $N_{phels}(E)$ on energy, see Figs. 5 and 6. However, $N_{phels}(E)$ is about 30% smaller than

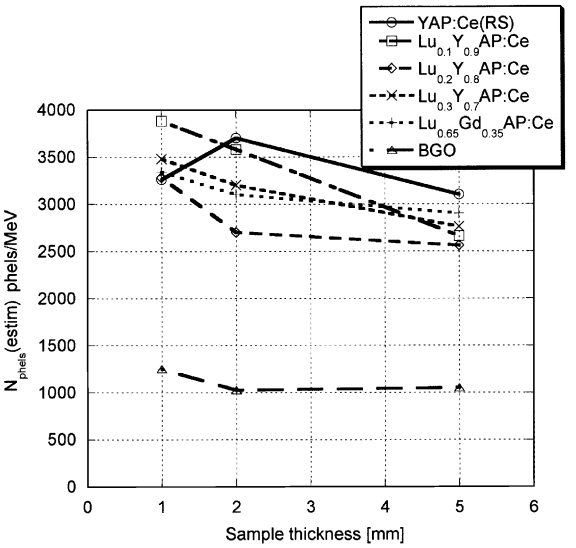

Fig. 12. Total N_{phels}(estim) yield at 1 MeV energy versus sample thickness for different perovskite crystals. Values for BGO multiplied by a correction factor of 1.25 are also shown.

the values for the best $YAlO_3$:Ce crystals (see Tables 1 and 2) and $N_{phels}(E)$ decrease with sample thickness, see Fig. 12. This decrease is smaller for $Lu_xGd_{1-x}AlO_3$:Ce than for $Lu_xY_{1-x}AlO_3$:Ce crystals. Their Stokes shifts, see Table 5, are not the same. At present we have no explanation for the small Stokes shift of $Lu_{0.3}Y_{0.7}AlO_3$:Ce compared with other crystals investigated, see Table 4.

4.3. Comparison of $N_{phels}(E)$ yields between different Ce^{3+}-doped perovskite crystals

The use of scintillators for γ-ray imaging applications like in the γ-imaging camera or PET systems increases [16–19,22,23]. Some of these systems use multi-crystal detectors composed from small $YAlO_3$:Ce blocks (pixels) of about $1 \times 1 \times 10\,mm^3$ dimensions [17,19,20]. In these multi-crystal detectors detailed studies of light collections are necessary as for example provided by Vittori et al. [33] or Saoudi et al. [34]. In these multi-detectors, the photon CE depends on the length and cross-sectional area of $YAlO_3$:Ce pixels. The shortest decrease in the efficiency was observed for pixels of 2×2 cross-section [33] and the efficiency decrease is $\approx 30\%$ for pixels of length between 1 and 10 mm while for pixels of $0.3 \times 0.3\,mm^2$ cross-section and the same length the decrease is almost 60% Generally, LY and energy resolutions of individual crystal pixels and those of the whole multi-crystal detector can be influenced by light absorption and scattering in the individual crystals or in the whole multi-detector.

$N_{phels}(E)$ yields of $YAlO_3$:Ce and other Ce^{3+}-doped perovskites decrease with sample thickness, see Fig. 12. The same was also observed for the BGO crystals applied in PET systems [25]. The decrease of N_{phels}(estim) yield of $YAlO_3$:Ce(RS) and $Lu_xY_{1-x}AlO_3$:Ce ($x = 0.1-0.3$) crystals when the thickness increases from 1 to 5 mm is about 18–22%. For $Lu_{0.65}Gd_{0.35}AlO_3$:Ce and BGO this decrease is between 12% and 13%. This confirm recent results of relative light yield studies in Ref. [5] where the influence of self-absorption was demonstrated for $YAlO_3$:Ce(RS) and $Lu_xY_{1-x}AlO_3$:Ce crystals but for $Lu_{0.65}Gd_{0.35}AlO_3$:Ce and BGO crystals self-absorption is probably less important.

Possible effects of self-absorption on $N_{phels}(E)$ or LY(E) yields of Ce^{3+}-doped perovskites is also demonstrated by the laser excited Ce^{3+} emission spectra, see Section 3.3 and Figs. 9 and 10. It is caused by the spectral overlaps between f→d absorption and d→f emission in the range 320–350 nm, but no large differences between crystals were observed. The emission spectrum of $Lu_{0.65}Gd_{0.35}AlO_3$:Ce crystal is somewhat shifted to longer wavelengths compared with that of $Lu_{0.3}Y_{0.7}AlO_3$:Ce. The measurements of the laser excited emission spectra on the 10 mm long $YAlO_3$:Ce SKB crystal, see Fig. 9, show not more than $\approx 11\%$ light loss due to self-absorption. From the transmission spectra of the 1 and 10 mm thick samples in Fig. 11 a light loss of roughly 20% is estimated. $N_{phels}(E)$ yields and the LY values of the $YAlO_3$:Ce SKB crystal in Table 4 show $\approx 30\%$ decrease with sample thickness increasing from 1 to 10 mm. This

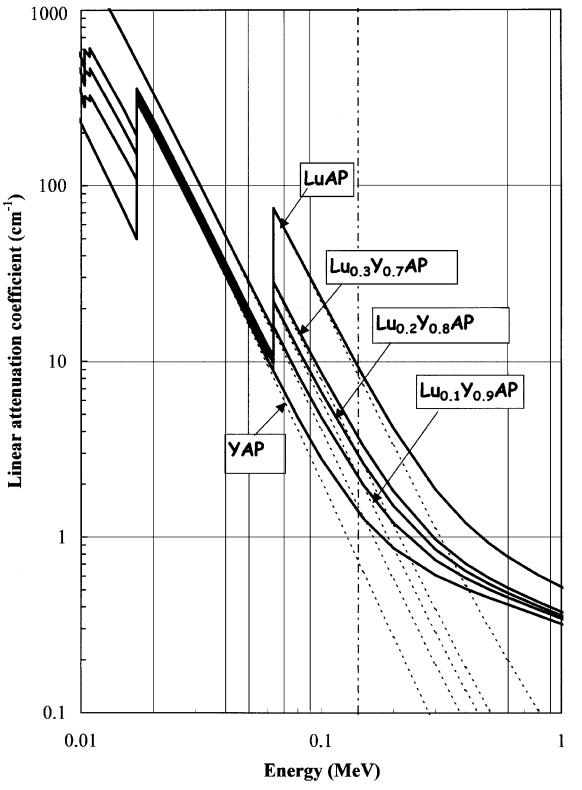

Fig. 13. Linear γ- and X-ray attenuation coefficients of $YAlO_3$, $Lu_xY_{1-x}AlO_3$:Ce ($x = 0.1$, 0.2, and 0.3) and $LuAlO_3$:Ce in the energy range 0.01–1 MeV.

Table 6
Properties of Ce^{3+}-doped perovskite crystals (some data were taken from papers [5,15])

Crystal	Density (g/cm^3)	τ_{sc} (ns)	Z_{eff}	N_{phels} for 122 keV 1 mm	$\Delta N_{phels}(ave)$ slopes in (phels/keV)	Lin. att. coeff. at 140 keV (cm^{-1})
YAP:Ce(RS)	5.36	25–30	34	≈199.2	1.63	1.3
YAP:Ce Zr (YAP4)	5.36	24	34	≈327.6	2.7	1.3
YAP:Ce,Zr(YAP11)	5.36	<20	34	≈276.9	2.25	1.3
$Lu_{0.1}Y_{0.9}$AP:Ce	5.73	18–25	43	236.9	1.94	2.0
$Lu_{0.2}Y_{0.8}$AP:Ce	5.92	18–25	49	200.6	1.64	2.6
$Lu_{0.3}Y_{0.7}$AP:Ce	6.19	17–22	53	213.4	1.74	3.3
$Lu_{0.6}Y_{0.4}$AP:Ce	7.84	20–30 or ⩾100	62	180.3	1.48	—
$Lu_{0.65}Y_{0.35}$AP:Ce	7.93	20–30 or ⩾100	63	205.3	1.68	—
LuAP:Ce	8.34	17–20	65	—	—	9.4

decrease is not caused by the self-absortpion only as it contributes ≈11%.

Besides perovskites, also a BGO crystal was investigated. Its $N_{phels}(E)$ yields are smaller than those of the perovskites. $N_{phels}(E)$ exhibits a linear dependence on energy in range 5–500 keV and it also decreases with sample thickness, see Fig. 12.

The linear attenuation coefficients $\mu(E)$ for γ-ray absorption has been calculated [35–37] for $YAlO_3$:Ce, $Lu_xY_{1-x}AlO_3$:Ce and $LuAlO_3$:Ce crystals and are presented in Fig. 13. Values of $\mu(E)$ at the 140 keV γ-ray line of the ^{99}Tc isotope used in nuclear medicine are given in the last column of Table 6. With the increase of Lu content μ(140 keV) increases from ≈1.3 cm^{-1} for $YAlO_3$:Ce to ≈9.4 cm^{-1} for $LuAlO_3$:Ce. Table 6 further compiles parameters like density, Z_{eff}, $N_{phels}(E)$, etc.

Another important parameter of scintillators like the Stokes shift ΔS measured at $T = 77$ K are given in Table 5. ΔS changes from ≈4130 to ≈2875 cm^{-1}. The difference of about 242 cm^{-1} between $YAlO_3$:Ce and $LuAlO_3$:Ce is small compared with the difference of 1006 cm^{-1} between $LuAlO_3$:Ce and $Lu_{0.3}Y_{0.7}AlO_3$:Ce. However, the largest effect of self-absorption was observed on $LuAlO_3$:Ce [9] and not on $Lu_{0.3}Y_{0.7}$Al-O_3:Ce. We have no clear explanation.

Important results were obtained on newly grown Zr co-doped $YAlO_3$:Ce crystals [32]. Their $N_{phels}(E)$ yields in Table 1 can be up to 60% higher than those of formerly grown $YAlO_3$:Ce crystals. Another important property of these samples is a shortening of their scintillation decay lifetimes from ≈28 ns in the YAP1 sample without Zr co-doping to 18 ns lifetime in the YAP11 sample [32]. The lifetime shortening could be especially, important for applications in PET systems or electron microscopy.

5. Conclusions

Scintillation photoelectron light yields are influenced by many different factors like sizes of samples, whether surfaces are polished or ground, type of reflection tape covering the samples, the interfaces between crystal and PMT or HPMT windows, etc. Also these scintillation properties can be influenced by the scintillation emission spectra and different photo-cathode quantum efficiency of the used PMT or HPMT [25,33,34]. Our main conclusions from detailed scintillation and spectroscopic investigations of Ce^{3+}-doped perovskite crystals are:

1. The γ-ray linear attenuation coefficient of $LuAlO_3$:Ce is almost 10 times higher than that of $YAlO_3$:Ce. In the energy range 5 keV to 1 MeV $N_{phels}(E)$ yields increase linearly with energy E, see Figs. 4–6.

2. When Zr is used as co-dopant, $N_{phels}(E)$ yields of $YAlO_3$:Ce increase up to 60% and the Ce^{3+} scintillation decay lifetime shortens to below 20 ns [32], see Table 1 and Fig. 7. When sample thickness increases from 1 or 2 to 10 mm the yield of $YAlO_3$:Ce samples decrease by 30%.
3. The self-absorption is the smallest for the $YAlO_3$:Ce SKB samples. It is about 11% for a 10 mm long crystal. In 5 mm thick $Lu_{0.3}Y_{0.7}AlO_3$:Ce and $Lu_{0.65}Gd_{0.35}AlO_3$:Ce self-absorption is $\approx$11.6 and $\approx$16.7%, respectively. Note that in $LuAlO_3$:Ce self-absorption is 60% for a sample of 10 mm thick [9,38]. A clear relation between self-absorption and the Stokes shift ΔS was not established.
4. For accurate determination of $N_{phels}(E)$ yields and $LY(E)$ measurements should preferably be carried out on 10 mm diameter and 1 mm thick samples with polished both faces and grounded walls as was formerly recommended by Moszynski et al. [25].
5. Optimized $YAlO_3$:Ce crystals exhibit LY up to 25,000 ph/MeV and transmission properties exceed those of $Lu_xY_{1-x}AlO_3$:Ce or $Lu_xGd_{1-x}AlO_3$:Ce.

$YAlO_3$:Ce and $YAlO_3$:Ce, Zr exhibit the best crystal growing and light yield properties for the use in medical imaging detectors. The main disadvantage is the relatively low density $\rho = 5.36\,g/cm^3$. Due to the absence of intense slow decay components $Lu_xY_{1-x}AlO_3$:Ce crystals exhibit higher linear attenuation coefficients for γ-radiation than $YAlO_3$:Ce especially for used 140 keV γ-ray line of ^{99}Tc.

Especially, $Lu_{0.3}Y_{0.7}AlO_3$:Ce could be used as $\approx$2 mm thick scintillating window for the improved hybrid photo-multiplier tubes or as the pixels in multi-detectors. These crystals together with $YAlO_3$:Ce exhibit also lower self-absorption compared with pure $LuAlO_3$:Ce crystals. Future development and applications of mixed or heavy perovskites will depend on technological achievements and improvements together with better commercial availability of raw materials, especially Lu_2O_3.

Acknowledgements

Support of NATO SfP 973510—Scintillators Project is gratefully acknowledged, especially for the development of $YAlO_3$:Ce,Zr crystals. R. Calzolai from IFAC-CNR in Florence is gratefully acknowledged for optical treatment of crystals. We appreciate the support of the Grant Agency of the Czech Republic (Grant GA CR 202/01/0753) and of the Ministry of Education of the Czech Republic (MSMT Kontakt ME462 Grant). Mixed $Lu_x(RE)_{1-x}AP$:Ce crystals were developed under the Institutional Partnership research program of the Swiss National Science Foundation, grant 71P051218 in the years 1997–1999.

References

[1] M. Kapusta, M. Moszynski, M. Balcerzyk, J. Braziewicz, D. Wolski, J. Pawelke, W. Klamra, IEEE Trans. Nucl. Sci. NS-47 (2000) 1341.
[2] M. Nikl, Phys. Status Solidi (A) 178 (2000) 595.
[3] J.A. Mares, N. Cechova, M. Nikl, J. Kvapil, R. Kratky, J. Alloys Compounds 275–277 (1998) 200.
[4] J.A. Mares, M. Nikl, J. Chval, J. Giba, K. Nejezchleb, D. Clement, J.-F. Loude, C. Morel, Rad. Eff. Def. Solids 150 (Part II) (1999) 59.
[5] J. Chval, D. Clement, J. Giba, J. Hybler, J.-F. Loude, J.A. Mares, E. Mihokova, C. Morel, K. Nejezchleb, M. Nikl, A. Vedda, H. Zaidi, Nucl. Instr. and Meth. A 443 (2000) 331.
[6] C. Dujardin, C. Pedrini, W. Blanc, J.C. Gacon, J.C. van't Spijker, O.W.V. Frijns, C.W.E. van Eijk, P. Dorenbos, R. Chen, A. Fremout, F. Tallouf, S. Tavernier, P. Bruyndonckx, A.G. Petrosyan, IEEE Trans. Nucl. Sci. NS-45 (1998) 467.
[7] M. Nikl, E. Mihokova, J.A. Mares, A. Vedda, M. Martini, K. Nejezchleb, K. Blazek, Phys. Status Solidi (b) 181 (2000) R10 (Rapid research note).
[8] P. Dorenbos, M. Marsman, C.W.E. van Eijk, in: P. Dorenbos, C.W.E. van Eijk (Eds.), Proceedings of the International Conference on Inorganic Scintillators and their Applications, SCINT 95, Delft University Press, The Netherlands, 1996, p. 148.
[9] C. Dujardin, C. Pedrini, W. Blanc, J.C. Gacon, J.C. van't Spijker, O.W.V. Frijns, C.W.E. van Eijk, P. Dorenbos, R. Chen, A. Fremont, F. Tallouf, S. Tavernier, P. Bruyndonckx, A.G. Petrosyan, J. Condens. Matter 10 (1998) 3061.
[10] H. Suzuki, T.A. Tombrelo, C.L. Meltzer, J.S. Schweitzer, IEEE Trans. Nucl. Sci. NS-40 (1993) 380.
[11] C.W.E. van Eijk, Nucl. Instr. and Meth. A 460 (2001) 1.

[12] E.V.D. van Loef, P. Dorenbos, C.W.E. van Eijk, K. Kramer, H.U. Gudel, Appl. Phys. Lett. 79 (2001) 1573.
[13] E.V.D. van Loef, P. Dorenbos, C.W.E. van Eijk, K. Kramer, H.U. Gudel, Appl. Phys. Lett. 77 (2000) 1467.
[14] P. Dorenbos, Nucl. Instr. and Meth. A 486 (2002) 208.
[15] P. Lecoq, in: V.V. Mikhailin (Ed.), Proceedings of the International Conference on Inorganic Scintillators and Their Applications, SCINT 99, Moscow St. University, Russia, 2000, p. 3.
[16] A.G. Weisenberger, S. Majewski, M. Saha, E. Bradley, Nucl. Instr. and Meth. 392 (1997) 299.
[17] R. Pani, F. de Notaristefani, K. Blazek, P. Maly, R. Pellegrini, A. Pergola, A. Soluri, F. Scopinario, Nucl. Instr. and Meth. A 348 (1994) 551.
[18] R. Amendolia, E. Bertolucci, et al., Nucl. Instr. and Meth. A 442 (1999) 201.
[19] A. Del Guerra, M.G. Bisogni, C. Damiani, G. Di Domenico, R. Marchesini, G. Zavattini, Nucl. Instr. and Meth. A 442 (2000) 18.
[20] C. D'Ambrosio, F. De Notaristefani, T. Gys, H. Leutz, D. Piedigrossi, D. Puertolas, E. Rosso, Nucl. Instr. and Meth. A. 442 (2000) 279.
[21] CMS TDR, ALICE TDR, CERN, Geneve, 1999–2000.
[22] R. Pani, R. Pellegrini, F. Scopinario, A. Soluri, G. De Vincentis, A. Pergola, F. Iacopi, A. Corona, A. Grammatico, S. Filipi, P.L. Ballesio, Nucl. Instr. and Meth. A 392 (1997) 295.
[23] S. Majewski, F. Farzanpay, A. Goode, B. Kross, D. Steinbach, A. Weisenberger, M. Williams, R. Wojcik, Nucl. Instr. and Meth. A 409 (1998) 520.
[24] M. Balcerzyk, Z. Gontarz, M. Moszynski, M. Kapusta, J. Lumin. 87-89 (2000) 963.
[25] M. Moszynski, M. Kapusta, M. Mayhugh, D. Wolski, S.O. Flyck, IEEE Trans. Nucl. Sci. NS-44 (1997) 1052.
[26] C. D'Ambrosio, F. De Notaristefani, H. Leutz, D. Puertolas, E. Rosso, IEEE Trans. Nucl. Sci. NS-47 (2000) 6.
[27] C. D'Ambrosio, F. De Notaristefani, H. Leutz, D. Puertolas, E. Rosso, Nucl. Instr. and Meth. A 431 (1999) 445.
[28] E. Barni, G. Viscardi, C. D'Ambrosio, H. Leutz, D. Puertolas, S. Tailhart, P. Destruel, P. Jolinat, H. Gusten, Appl. Spectrosc. 51 (1997) 1193.
[29] C. D'Ambrosio, C. Ercoli, S. Jaaskelainen, G. Lecoeur, H. Leutz, E. Rosso, R. Shomaker, Nucl. Instr. and Meth. A 434 (1999) 387.
[30] C. D'Ambrosio, C. Ercoli, S. Jaaskelainen, E. Rosso, P. Wicht, Nucl. Instr. and Meth. A 388 (1997) 119.
[31] J.A. Mares, J. Alloys Compounds 300–301 (2000) 95.
[32] M. Nikl, J.A. Mares, J. Chval, E. Mihokova, M. Martini, A. Vedda, K. Blazek, P. Maly, K. Nejezchleb, P. Fabeni, G.P. Pazzi, V. Babin, K. Kalder, A. Krasnikov, S. Zazubovich, C. D'Ambrosio, Nucl. Instr. and Meth. A 486 (1–2) (2002) 250.
[33] F. Vittori, F. de Notaristefani, T. Malatesta, D. Puertolas, Nucl. Instr. and Meth. A 452 (2000) 245.
[34] A. Saodi, C.M. Pepin, R. Lecomte, IEEE Trans. Nucl. Sci. NS-47 (2000) 1634.
[35] E. Storm, H. Izrael, Photon cross sections from 0.001 to 100 MeV for elements 1 through 100, Los Alamos Scientific Laboratory, New Mexico, USA, June 1967.
[36] WWW pages of the Centre for X-ray Optics, Materials Sciences Divisions of LBNL, CA, USA, 2002 (http://www.cxro.lbn.gov).
[37] W.R. Leo, Techniques for Nuclear and Particle Physics Experiments, 2nd Edition, Springer, Berlin, Heidelberg, New York and other towns, 1994, pp. 62–63.
[38] R. Pani, R. Scafe, R. Pellegrini, A. Soluri, G. Trotta, L. Indovina, M.N. Cinti, G. De Vincentis, Nucl. Instr. and Meth. A 477 (2002) 72.